



## CENTRE DE RECERCA MATEMÀTICA

This is a preprint of: *Stochastic modelling of the eradication of the HIV-1 infection by stimulation of latently infected cells in patients under highly active anti-retroviral therapy*

Journal Information: *Journal of Mathematical Biology*,

Author(s): D. Sanchez-Taltavull, A. Vieiro, T. Alarcon.

Volume, pages: 73(4) 1-28, DOI:[10.1007/s00285-016-0977-5]



# Stochastic modelling of the eradication of the HIV-1 infection by stimulation of latently infected cells in patients under highly active anti-retroviral therapy

Daniel Sánchez-Taltavull<sup>1,4</sup> · Arturo Vieiro<sup>2</sup> ·  
Tomás Alarcón<sup>3,4,5,6</sup>

Received: 15 December 2014 / Revised: 8 December 2015 / Published online: 26 February 2016  
© Springer-Verlag Berlin Heidelberg 2016

**Abstract** HIV-1 infected patients are effectively treated with highly active anti-retroviral therapy (HAART). Whilst HAART is successful in keeping the disease at bay with average levels of viral load well below the detection threshold of standard clinical assays, it fails to completely eradicate the infection, which persists due to the emergence of a latent reservoir with a half-life time of years and is immune to HAART. This implies that life-long administration of HAART is, at the moment, necessary for HIV-1-infected patients, which is prone to drug resistance and cumulative side effects as well as imposing a considerable financial burden on developing countries, those more afflicted by HIV, and public health systems. The development of therapies which specifically aim at the removal of this latent reservoir has become a focus of much research. A proposal for such therapy consists of elevating the rate of activation of

---

✉ Daniel Sánchez-Taltavull  
dsanchez@crm.cat; dsancheztaltavull@ohri.ca

Arturo Vieiro  
vieiro@maia.ub.es

Tomás Alarcón  
talarcon@crm.cat

- <sup>1</sup> Regenerative Medicine Program, Ottawa Hospital Research Institute, Ottawa K1H 8L6, Canada
- <sup>2</sup> Departament de Matemàtica Aplicada i Anàlisi, Universitat de Barcelona, 08007 Barcelona, Spain
- <sup>3</sup> ICREA (Institució Catalana de Recerca i Estudis Avançats), Barcelona, Spain
- <sup>4</sup> Centre de Recerca Matemàtica, Edifici C, Campus de Bellaterra, Bellaterra, 08193 Barcelona, Spain
- <sup>5</sup> Departament de Matemàtiques, Universitat Autònoma de Barcelona, Bellaterra, 08193 Barcelona, Spain
- <sup>6</sup> Barcelona Graduate School of Mathematics (BGSMath), Barcelona, Spain

the latently infected cells: by transferring cells from the latently infected reservoir to the active infected compartment, more cells are exposed to the anti-retroviral drugs thus increasing their effectiveness. In this paper, we present a stochastic model of the dynamics of the HIV-1 infection and study the effect of the rate of latently infected cell activation on the average extinction time of the infection. By analysing the model by means of an asymptotic approximation using the semi-classical quasi steady state approximation (QSS), we ascertain that this therapy reduces the average life-time of the infection by many orders of magnitudes. We test the accuracy of our asymptotic results by means of direct simulation of the stochastic process using a hybrid multi-scale Monte Carlo scheme.

**Keywords** HIV-1 · HAART · Latently infection · Stochastic modelling · Antigen stimulation

**Mathematics Subject Classification** 34E20 Singular perturbations, turning point theory, WKB methods · 34E13 Multiple scale methods · 92B05 General biology and biomathematics

## 1 Introduction

Quantitative analysis of the temporal evolution of plasma viral load upon administration of HAART indicates the existence of several phases in the decay of the viral load (Pierson et al. 2000; Kim and Perelson 2006; Jones and Perelson 2007; Rong and Perelson 2009). After an initial shoulder, due to delays associated to both the pharmacokinetics and the production of virus by newly infected cells (Perelson et al. 1996; Herz et al. 1996), a first phase of fast exponential decline of the viral load ensues whereby the viral load is reduced by up to two orders of magnitude over a period of time of approximately two weeks. This fast response stage, with half-life time of several days, reflects short half-life time of plasma virus and of productively infected CD4<sup>+</sup> T lymphocytes (Ho et al. 1995; Wei et al. 1995; Markowitz et al. 2003). Following this initial phase, a second stage of slower decay starts with a half-life between one and four weeks. This phase is associated to the contribution to virus load of infected cells with longer half-life time, such as macrophages, and infected CD4<sup>+</sup> T cells that exhibit a lower rate of viral replication (Perelson et al. 1997; Ho et al. 1986; Zhang et al. 1999). After this second stage, plasma virus load has normally fallen below the detection threshold of standard clinical assays ( $\sim 50$  copies RNA/ml). However, following this second phase, HAART appears to fail to completely eradicate the infection. Rather, a third stage ensues with much longer half-life time than the previous ones (of the order of months or even years Kim and Perelson 2006) in which residual levels of viral load (1–5 copies RNA/ml detectable only by supersensitive assays) persist in plasma as well as in other bodily compartments, such as semen.

The issue of what is the source of this residual viral load has triggered much debate that has crystallised in several working hypotheses. One of these hypotheses invokes the possibility that HAART is not completely suppressive thus allowing the infection to continue to replicate in anatomical HIV-1 reservoirs (Pierson et al. 2000),

in particular within the so-called “drug sanctuaries”, i.e. sites poorly penetrated by the drug where the infection persists (Kepler and Perelson 1998). An alternative model suggests that, although HAART could be fully suppressive, a cellular reservoir exists that allows the infection to linger in latent form (Pierson et al. 2000), the residual viral load being the result of the activation of the latently infected cells (Pierson et al. 2000). Such a latent reservoir is established within the population of infected CD4+ T memory cells (Chun et al. 1995, 1997). They therefore stay in their resting state in the presence of HAART for prolonged periods of time. The latently infected cell population is replenished by both active infected cell proliferation and also by slow, density-dependent homeostatic proliferation of the memory CD4+ T memory cells (and, therefore, of the latently infected cell compartment), which, according to Chomont et al. (2009), drives persistence and determines the size of the latent reservoir. This cycle is able to maintain positive, although rather small levels of viral load for very long time. Latently infected cells are thus able to escape the effect of the drug and immune surveillance due to the fact that they undergo duplication at very low rates and, consequently, exhibit very low levels of HIV-1 messenger RNA (Rong and Perelson 2009). However, since latently infected cells release virus when stimulated with the proper antigen, viral rebound will eventually occur when HAART is withdrawn leading to HIV-1 infection recurrence, consistent with a wider scenario of quiescence-induced escape (Alarcón and Jensen 2011).

The presence of this latent infection has been recognised as a major barrier for complete eradication of HIV-1 infection and the search for combination therapies, i.e. HAART plus specific agents that tackle the latent reservoir, has become a focus of research in HIV therapeutics (Trono et al. 2010; Shan et al. 2012; Katlama et al. 2013; Kent et al. 2013). One of such potential approaches consists of using agents that activate latently infected cells: by activating the cells in the latent reservoir, they would be rendered sensitive to the anti-retroviral drugs since activation implies onset of virus production. This would, at least theoretically, clear the latent reservoir and, eventually, the infection. Early studies regarding activation of the latent reservoir used interleukins (IL-2, IL-3, and IL-7) in combination with specific antibodies (CD3). These attempts failed because these interleukins were found to increase the absolute count of T cells (Trono et al. 2010; Shan et al. 2012). More recent studies have focused on the use of small molecules that reactivate latent virus production without inducing global T cell activation, in particular several histone deacetylases (HDAC) and other chromatin modifiers (Trono et al. 2010). The aim of this paper is to use a stochastic model of the HIV-1 infection in an individual patient treated to assess the feasibility and efficiency of activation of latently infected cells in combination of HAART. In particular, our aim is to analyse how the average extinction time of the infected cell population (both active and latent) changes as the activation rate of latently infected cells is increased. We also evaluate possible side effects such as the increase in viral load following latently infected cell activation.

Our analysis proceeds by means of a WKB asymptotic analysis of the partial differential equation for the probability generating function associated to the Master Equation which describes stochastic infection dynamics. This method relies on the solution of a variational problem for the optimisation of an action functional, which effectively reduces the problem to the analysis of the associated Hamilton equations

(Kubo et al. 1973; Alarcón and Page 2007; Elgart and Kamenev 2004). In order to progress further, we take advantage of the multiplicity of time scales in the system to perform a quasi-steady state approximation (QSSA) on the Hamilton equations, thus reducing the dimensionality of the problem (Alarcón 2014; de la Cruz et al. 2014). We further use advanced numerical techniques to analyse the multi-dimensional Hamiltonian system: computation of invariant manifolds (Simó 1990; Haro et al. 2016) and the Taylor integration method (Jorba and Zou 2005) together with automatic differentiation techniques (Jorba and Zou 2005), which are used to obtain high accuracy with larger time steps. Our asymptotic and numerical results are tested by means of multi-scale stochastic simulations (Cao et al. 2005).

The organisation of the paper is as follows. Section 2 is devoted to presenting our model of the HIV-1 dynamics under HAART in detail and discussing its underlying hypotheses. In Sect. 3, we present an asymptotic analysis of our stochastic model, which transforms it into a classical mechanics problem via the application of the semi-classical approximation to the PDE for the generating function associated to the probability distribution. In Sect. 4, we present our results regarding effectiveness and feasibility of the combination of HAART and latently infected cell activation therapy. In Sect. 5, we summarise our results and present our conclusions. Additionally, 3 appendixes are included to give all the mathematical details of the different techniques used in the paper. In “Appendix 1”, we perform a time-scale analysis of our system, and we use it to reduce our Hamiltonian system to a simpler Hamiltonian problem with 1 or 2 degrees of freedom. In “Appendix 1” we introduce the different techniques used compute invariant manifolds and heteroclinic connections necessary to calculate the average extinction time of our stochastic problem. In “Appendix 1” we present a procedure to estimate numerically some parameters of the expression of the average extinction time.

## 2 Formulation of the stochastic model

Our model is a stochastic generalisation of the model proposed by Rong and Perelson (2009) and the model presented by Conway and Coombs (2011). It takes into account the stochastic evolution of four variables,  $(T, L, T^*, V)$ , namely, the number of CD4<sup>+</sup> T-cells that are susceptible to HIV-1 infection, the number of latently infected cells, the number of productively infected cells and the viral load. Whilst only  $T^*$ -cells can produce and release virus,  $L$ -cells can be activated by their recall antigens and become actively infected cells.

Our stochastic model of viral dynamics is schematically shown in Fig. 1. We assume that, upon infection of an uninfected T cell, two types of infected cells can emerge, namely, latently infected cells,  $L$ , and active infected cells,  $T^*$ . Active infected cells are targeted by HAART whereas latently infected cells are immune to its effects. Furthermore, latently infected cells can become active, for example, by stimulation with appropriate antigens. Both latently and active infected cells are assumed to die at a certain rate and blood-borne virions are assumed to be cleared off at a constant rate. Actively infected cells synthesise and release virions which infect susceptible T cells at a rate which depends on HAART effectiveness,  $\epsilon$ . Although previous evi-

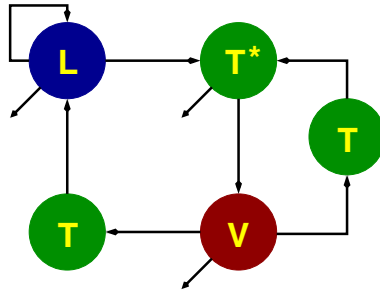


**Fig. 1** Schematic representation of the stochastic infection model whose dynamics is determined by the transition rates reported in Table 1: virions ( $V$ ), which are produced by active infected cells ( $T^*$ ), infect T cells ( $T$ ) thus producing latently ( $L$ ) and active infected cells. Latently infected cells can be activated thus becoming active infected cells. Both types of infected populations decay by cell death whilst viral load decays due to virion clearance. We further assume that the latently infected population undergoes density-dependent homeostatically regulated proliferation. See Sect. 2 for a full description of the stochastic infection dynamics

dence, reported in Siliciano et al. (2003), according to which the latent reservoir is decaying, we incorporate into our model that the latently infected cells are maintained by homeostatic proliferation, as suggested by more recent experimental results (Chomont et al. 2009). This is accomplished by means of a phenomenological model which includes branching and binary annihilation of latently infected cells (Rong and Perelson 2009; Elgart and Kamenev 2004). We consider this scenario, where an steady, positive latently infected population exists, as it represents the least favourable scenario against which to test the effectiveness and feasibility of the combined therapy we study in this paper.

Within the framework of this model, we focus on the analysis of the effect on the system of latently infected cell stimulation therapy (LICST). To this end, we study how the system's behaviour is altered as the key parameter  $a_L$ , i.e. the rate of activation of the latently infected cells, varies. In particular, we analyse the dependence of the average extinction time of the HIV infection under the combined action of HAART and LICST. In order to proceed with this programme, we formulate our stochastic model in terms of the associated master equation (Van Kampen 2007; Gardiner 2009):

$$\frac{\partial P(X, t)}{\partial t} = \sum_j (W_j(X - r_j, t)P(X - r_j, t)) - W_j(X, t)P(X, t) \quad (1)$$

where  $X = (x_1, x_2, x_3, x_4) = (T, L, T^*, V)$  and  $P(X, t)$  is the probability of the state vector to be equal to  $X$  at time  $t$ . For full specification of our stochastic model, we need to prescribe the transition rates,  $W_j(X, t)$ , associated to the probability per unit time of the elementary processes  $j$  to occur. We follow the standard modelling strategy whereby these rates are modelled by means of the law of mass action (Gillespie 1976). Moreover, the quantities  $r_j$  are the change in the state vector,  $X$ , when elementary process  $j$  occurs, i.e.  $X(t + \Delta t) = X(t) + r_j$  with probability  $W_j \Delta t = P(X(t + \Delta t) = X(t) + r_j | X(t))$ .

The elementary processes involved in our model are (see Table 1):

**Table 1** Transition rates corresponding to the stochastic model of HIV infection dynamics

| Transition rate  | $r_j = (\Delta T, \Delta L, \Delta T^*, \Delta V)$ | Description  |
|--|--|--|
| $W_1 = \lambda \Omega$                                   | $(1, 0, 0, 0)$                                     | Recruitment of $T$ cells: $\emptyset \rightarrow T$                          |
| $W_2 = d_T T$  | $(-1, 0, 0, 0)$                                    | Death of uninfected cells: $T \rightarrow \emptyset$                         |
| $W_3 = \eta(1 - \epsilon)kVT\Omega^{-1}$                 | $(-1, 1, 0, -1)$                                   | Infection: $T + V \rightarrow L$   |
| $W_4 = (1 - \eta)(1 - \epsilon)kVT\Omega^{-1}$           | $(-1, 0, 1, -1)$                                   | Infection: $T + V \rightarrow T^*$   |
| $W_5 = rL$   | $(0, 1, 0, 0)$                                     | $L$ -cell homeostatic proliferation:<br>$L \rightarrow 2L$                   |
| $W_6 = \frac{r}{L_{max}} \frac{L^*(L-1)}{2} \Omega^{-1}$ | $(0, -2, 0, 0)$                                    | $L$ -cell homeostatic annihilation:<br>$L + L \rightarrow \emptyset$         |
| $W_7 = d_0 L$  | $(0, -1, 0, 0)$                                    | Death of latently infected cells:<br>$L \rightarrow \emptyset$               |
| $W_8 = a_L L$  | $(0, -1, 1, 0)$                                    | Activation of $L$ -cells: $L \rightarrow T^*$                                |
| $W_9 = \delta T^*$                                       | $(0, 0, -1, 0)$                                    | Death of actively infected cells:<br>$T^* \rightarrow \emptyset$             |
| $W_{10} = cV$  | $(0, 0, 0, -1)$                                    | Virus clearance: $V \rightarrow \emptyset$                                   |
| $W_{11} = p_v T^*$                                       | $(0, 0, 0, 1)$                                     | Production of virus by actively<br>infected cells: $T^* \rightarrow T^* + V$ |
| $W_{12} = \epsilon kVT\Omega^{-1}$                       | $(0, 0, 0, -1)$                                    | Infection failed: $T + V \rightarrow T$                                      |

A description of the corresponding elementary population-dynamical processes is given in Sect. 2

- Recruitment of uninfected  $T$  cells with transition rate  $W_1$  (see Table 1). Uninfected  $T$  cells can further undergo death with transition rate  $W_2$  (see Table 1).
- Latently infected cells  $L$  can undergo:
  1. *Homeostatically-balanced proliferation* Following [Rong and Perelson \(2009\)](#), where density-dependent proliferation of  $L$ -cells was modelled in terms of a logistic growth, we account for homeostatic control of proliferation of the latently infected cell compartment by means of a combination of branching ( $L \rightarrow 2L$ ) with binary annihilation ( $L + L \rightarrow \emptyset$ ). It has been shown (see e.g. [Elgart and Kamenev 2004](#)) that this combination is a stochastic counterpart of the standard logistic growth. The associated transition rates are  $W_5$  for branching and  $W_6$  for binary annihilation (see Table 1).
  2. *Death* We assume a simple linear decay with transition rate  $W_7$  as shown in Table 1.
  3. *Activation* By means of this process, a latently infected cell can become an active infected cell  $L \rightarrow T^*$ . The corresponding transition rate is  $W_8$ , see Table 1.
- Active infected cells,  $T^*$ , are subjected to:
  1. Death with transition rate  $W_9$  (see Table 1).
  2. *Virion production* Contrary to latently infected cells, active infected cells synthesise and release new virions. Transition rate  $W_{11}$  (Table 1) corresponds to continuous production and release.
- Finally, virus,  $V$ , can:

1. Infect a healthy T cell producing a latently infected cell. In patients under HAART, the infection process is hindered by the presence of an anti-retroviral drugs. Following [Rong and Perelson \(2009\)](#), the efficiency of HAART is measured by a parameter,  $\epsilon$ , which takes values between 0 and 1, the latter (former) corresponding to a maximally (in)efficient drug.  $(1 - \epsilon)$  is interpreted as the proportion of virions capable of infection under HAART treatment. We also assume that, upon infection, the cell can become latently infected with probability  $\eta$  or active with probability  $(1 - \eta)$ . Therefore the corresponding transition rate  $W_3$  is proportional to  $\eta(1 - \epsilon)$  as shown in Table 1.
2. Infect a healthy T cell producing an active infected cell. In this case, the corresponding transition rate  $W_4$  is proportional to  $(1 - \eta)(1 - \epsilon)$  (see Table 1).
3. *Undergo clearance* Virions are removed from the blood, and we model this process as a simple linear decay with transition rate  $W_{10}$  as shown in Table 1.
4. Fail to infect and being eliminated by the drug with transition rate  $W_{12}$  (see Table 1).

**Parameter values** The (default) parameter values used in our simulations are summarised in Table 2. The parameter values corresponding to the model of cellular dynamics of an HIV-1-infected T-cell population with latency are based on estimates available in the literature on the subject. We will analyse the behaviour of the system as the value of the activation rate of the latently infected cells,  $a_L$ , varies.

**Mean-field dynamics** Although our aim is to analyse the effect of latently infected cell stimulation therapy on the average time of stochastic extinction of the HIV infection, it is often instructive to study the mean-field limit of the infection dynamics which is given by the following set of ordinary differential equations:

$$\frac{d}{dt}T(t) = \lambda - d_T T - (1 - \epsilon)kVT, \quad (2)$$

$$\frac{d}{dt}L(t) = \eta(1 - \epsilon)kVT + rL \left(1 - \frac{L}{L_{max}}\right) - d_0 L - a_L L, \quad (3)$$

$$\frac{d}{dt}T^*(t) = (1 - \eta)(1 - \epsilon)kVT - \delta T^* + a_L L, \quad (4)$$

$$\frac{d}{dt}V(t) = p_v T^* - cV - kVT. \quad (5)$$

The mean field limit corresponds to that regime where finite-size induced noise can be ignored. In other words, the mean field limit is associated to  $\Omega \rightarrow \infty$ . For this limit to be well defined, the reaction rates associated to the Master Equation,  $W_i(X, t)$ , must scale with system size in an appropriate manner. According to [Kubo et al. \(1973\)](#) and [Gillespie \(1976\)](#), a sufficient condition for this to be accomplished is that  $W_i(X, t) = \Omega w_i(x, t)$  where  $x = X/\Omega$ . The reaction rates and the associated rate constants are defined so that this condition is fulfilled and the mean field limit is well defined.

The mean-field system Eqs. (2)–(5) have two fixed points. The point with coordinates  $(T_1, 0, 0, 0)$ , i.e. the disease-free equilibrium associated to extinction of



**Table 2** Parameter values used in our numerical simulations

| Parameter  | Description   | Value                                     |
|------------|---|---|
| $T_0$      | CD4+ T cells at the metastable state                      | 599,999 cells ml <sup>-1</sup>            |
| $L_0$      | Latently infected cells at the metastable state           | 0.934778 cells ml <sup>-1</sup>           |
| $T_0^*$    | Productively infected cells at the metastable state       | 0.115067 cells ml <sup>-1</sup>           |
| $V_0$      | Viral load at the metastable state                        | 10 copies ml <sup>-1</sup>                |
| $T_1$      | CD4+ T cells at the extinction                            | 600,000 cells ml <sup>-1</sup>            |
| $L_1$      | Latently infected cells at the extinction                 | 0 cells ml <sup>-1</sup>                  |
| $T_1^*$    | Productively infected cells at the extinction             | 0 cells ml <sup>-1</sup>                  |
| $V_1$      | Viral load at the extinction                              | 0 copies ml <sup>-1</sup>                 |
| $\lambda$  | Recruitment rate of $T$ cells                             | 10,000 ml <sup>-1</sup> day <sup>-1</sup> |
| $d_T$      | Death rate of $T$ cells                                   | 0.0166 day <sup>-1</sup>                  |
| $k$        | Infection rate  | $2.4 \times 10^{-8}$ ml day <sup>-1</sup> |
| $\epsilon$ | Drug efficacy   | 0.85                                      |
| $\eta$     | Fraction resulting in latency                             | 0.001                                     |
| $d_0$      | Death rate of latently infected cells                     | 0.001 day <sup>-1</sup>                   |
| $a_L^s$    | Standard rate of transition from latently to productively | 0.1 day <sup>-1</sup>                     |
| $a_L^*$    | Critical value of $a_L$                                   | 0.199045 day <sup>-1</sup>                |
| $a_L$      | Rate of transition from latently to productively          | Varied                                    |
| $\delta$   | Death rate of productively infected cells                 | 1 day <sup>-1</sup>                       |
| $c$        | Clearance rate of free virus in blood stream              | 23 day <sup>-1</sup>                      |
| $p_v$      | Viral production rate                                     | 2000 day <sup>-1</sup>                    |
| $r$        | Proliferation rate of latent cells                        | 0.2 day <sup>-1</sup>                     |
| $L_{max}$  | Carrying capacity density of latent cells                 | 1.888 cells ml <sup>-1</sup>              |
| $\Omega$   | Dimensional system size                                   | 5000 ml                                   |
| $V_c$      | Typical volume of a human mammalian cell in culture       | 2000 $\mu\text{m}^3$                      |
| $N_c$      | Dimensionless system size                                 | $\Omega / V_c$                            |

the infection, is a repeller. The other fixed point, i.e. the positive equilibrium  $(y_1, y_2, y_3, y_4) \equiv (T_0, L_0, T_0^*, V_0)$  with  $L_0, T_0^*, V_0 \neq 0$ , is an stable fixed point (Rong and Perelson 2009). When noise is considered, the latter equilibrium becomes a metastable state, whereas the former becomes an absorbing state (Elgart and Kamenev 2004). In terms of the aims of this paper, we must study the behaviour of the mean-field

system as the activation rate of the latently infected cells,  $a_L$ , varies. From Eqs. (2)–(5), one checks that the positive equilibrium exists and is stable as long as  $a_L < a_L^*$ , where:

$$a_L^* = \frac{r - d_0}{1 - \left( \frac{\eta(1-\epsilon)kp_v T_1}{\delta(c+kT_1) - (1-\eta)(1-\epsilon)kp_v T_1} \right)}, \quad (6)$$

which implies that if latently infected cell activation is driven beyond the threshold set by  $a_L^*$ , the positive equilibrium disappears and the system is driven to extinction. Our analysis of the stochastic infection dynamics will reveal that this picture is incomplete. The linear stability analysis of the mean-field model predicts for values of the activation rate  $a_L < a_L^*$  a positive stable equilibrium exists and the trivial equilibrium (associated to extinction of the infection) is unstable. Therefore, within the mean-field scenario, extinction cannot occur if  $a_L < a_L^*$ . When noise is taken into account, extinction of the infection is possible even if  $a_L < a_L^*$ . Under these circumstances, the stable positive equilibrium becomes a metastable state of the stochastic dynamics and the trivial equilibrium, an absorbing state (which implies that eventual extinction occurs with probability one). To obtain a full picture, we must therefore analyse the dynamics of the stochastic dynamics of the infection. In particular, we will be interested in the average extinction time as function of  $a_L$ .

### 3 Model analysis: optimal fluctuation theory

In this section, we provide a description of the methods we use to analyse the stochastic infection dynamics described by Eq. (1) and, in particular, the asymptotic methods used to analyse the extinction dynamics. We follow the methodology presented in Alarcón (2014) and de la Cruz et al. (2014), i.e we analyse the system by means of a semi-classical quasi-steady state approximation (SCQSSA). We further check the accuracy of the predictions of our asymptotic analysis by means of a multi-scale stochastic simulation method, which takes advantage of the separation of time scales to produce fast simulations (Cao et al. 2005).

#### 3.1 Optimal fluctuation theory: semi-classical approximation and average extinction time

Our stochastic process is fully determined by  $P(x_1, x_2, x_3, x_4, t)$ , the solution of the Master Equation (1). This  $P(\mathbf{x}, t)$  has an associated generating function of the form

$$G(p_1, p_2, p_3, p_4, t) = \sum_{(x_1, x_2, x_3, x_4) \in \mathbb{N}^4} p_1^{x_1} p_2^{x_2} p_3^{x_3} p_4^{x_4} P(x_1, x_2, x_3, x_4, t). \quad (7)$$

In Sect. 3.1.1, we show that  $G(\mathbf{p}, t)$  can be approximated by

$$G(\mathbf{p}, t) \approx \exp(-N_c S_0(\mathbf{p}, t)),$$

where  $N_c$  is defined as the dimensionless parameter  $N_c \equiv \frac{\Omega}{V_c}$  which represents the system size.  $V_c$  is the average size of a  $T$  cell.

The quantity  $S_0$ , which is fully characterised in Eq. (12), is key to our approach, since following the theory of optimal fluctuation (i.e. the semi-classical approximation), provided that  $S_0 \gg 1$ , the average extinction time scales exponentially with  $S_0$  for the appropriate boundary conditions (Doering et al. 2005; Kamenev and Meerson 2008; Khasin and Dykman 2009).

Since extinction is the only absorbing state of the stochastic dynamics, and that state is reachable given any initial condition, extinction takes place with probability one. If the metastable state is of the form  $y_i \gg 0$ , which is associated to a system with size  $N_c \gg 1$ , the extinction probability  $P_0(t) = G(0, t)$  can be estimated by:

$$G(0, t) \approx 1 - \exp\left(-\frac{t}{\tau_E}\right), \quad (8)$$

where  $\tau_E$  is the average extinction time (see Assaf and Meerson 2007, 2006 for details).

### 3.1.1 Optimal fluctuation theory: semi-classical approximation

We now present the methodology we use to calculate the average extinction time, based on optimal fluctuation theory. This methodology, which we use to analyse the extinction dynamics of the stochastic infection model belongs to the wider class of WKB/large deviations methods (Kubo et al. 1973; Freidlin and Wentzell 1998). Similar approaches have been used to study extinctions in different contexts such as population models in ecology (Khasin and Dykman 2009; Assaf and Meerson 2010; Ovaskainen and Meerson 2010; Gottesman and Meerson 2012) and epidemiology (Dykman et al. 2008; Schwartz et al. 2009; Khasin et al. 2010). For reader's convenience we briefly summarised the main ideas. The following notation will be used: boldface  $\mathbf{v}$  denotes a vector of  $\mathbb{R}^4$  whose components are denoted by  $v_i$ ,  $i = 1, \dots, 4$ .

Let  $P(\mathbf{x}, t)$ ,  $\mathbf{x} \in \mathbb{N}^4$ , the probability distribution function related to the Markovian-process model considered. Denote by  $G(\mathbf{p}, t) = \sum_{\mathbf{x}=0}^{\infty} \mathbf{p}^{\mathbf{x}} P(\mathbf{x}, t)$  the associated generating function. The previous sum runs over the possible values of the variables  $x_i$  (positive quantities, in our system they account for the total number of each of the cells involved). Here  $\mathbf{p}$  is an auxiliary variable, below it will be interpreted as the momentum of an auxiliary Hamiltonian system describing the first order stochastic dynamics. The master Eq. (1) determines the evolution of  $G(\mathbf{p}, t)$ . In the particular case of our stochastic infection model with the reaction rates shown in Table 1, the corresponding partial differential equation for  $G(\mathbf{p}, t)$

$$\begin{aligned} \frac{\partial G}{\partial t} = & \lambda(p_1 - 1) + d_T(1 - p_1) \frac{\partial G}{\partial p_1} + (1 - \eta)(1 - \epsilon)k(p_3 - p_1 p_4) \frac{\partial^2 G}{\partial p_1 \partial p_4} \\ & + \eta(1 - \epsilon)k(p_2 - p_1 p_4) \frac{\partial G}{\partial p_1} \frac{\partial G}{\partial p_4} + r(p_2^2 - p_2) \frac{\partial G}{\partial p_2} + \frac{r}{2L_{\max}}(1 - p_2^2) \frac{\partial^2 G}{\partial p_2^2} \\ & + d_L(1 - p_2) \frac{\partial G}{\partial p_2} + a_L(p_3 - p_2) \frac{\partial G}{\partial p_2} + p_v(p_3 p_4 - p_3) \frac{\partial G}{\partial p_3} + \delta(1 - p_3) \frac{\partial G}{\partial p_3} \end{aligned}$$

$$+ c(1 - p_4) \frac{\partial G}{\partial p_4} + \epsilon k(p_1 - p_1 p_4) \frac{\partial^2 G}{\partial p_1 \partial p_4}. \quad (9)$$

The main idea to obtain an approximation of  $G(\mathbf{p}, t)$  is to use the classical Maupertuis principle of stationary abbreviated action. For Hamiltonian (time-independent) systems, Maupertuis' principle is equivalent to the the Hamilton's principle of stationary action since the abbreviated and Hamilton actions are related by a Legendre transformation. Moreover, the classical Hamilton's principle can be seen as the classical limit of the quantum stationary phase condition for constructive interference. We exploit these relations below, see [Goldstein \(1980\)](#), [Landau and Lifshitz \(1976\)](#), [Gray and Taylor \(2007\)](#) and [Gray et al. \(2004\)](#).

Equation 9 can be interpreted as a Schrödinger-like equation  $\frac{\partial}{\partial t} G = \hat{H} G$ , in terms of the (quantum) Hamiltonian operator  $\hat{H}$  expressed in the  $\hat{\mathbf{p}}$  (momentum) representation. Then  $\hat{q}_i \equiv \frac{\partial}{\partial \hat{p}_i}$ , and the operators  $\hat{p}_i$  and  $\hat{q}_i$  satisfy the commutation relation  $[\hat{q}_i, \hat{p}_j] = \delta_{i,j}$ . This relation motivates to express the solution of (9) as a Feynman path-integral representation, see for example ([Elgart and Kamenev 2004](#)):

$$G(\mathbf{p}, t) = \int_0^t \exp(-S(\mathbf{p}, \mathbf{q})) \mathcal{D}\mathbf{q}(s) \mathcal{D}\mathbf{p}(s) + \mathbf{p}_0^{\mathbf{x}}, \quad (10)$$

where  $S(\mathbf{p}, \mathbf{q})$  is the Hamilton action

$$S(\mathbf{p}, \mathbf{q}) = - \int_0^t \left( H(\mathbf{p}, \mathbf{q}) + \sum_{i=1}^n q_i(s) \dot{p}_i(s) \right) ds. \quad (11)$$

Here  $\mathcal{D}\mathbf{q}(s) \mathcal{D}\mathbf{p}(s)$  indicates integration over the space of all possible paths joining  $\mathbf{q}(0) = \mathbf{x}_0$  with  $\mathbf{p}(t) = \mathbf{p}_t$  fixed and  $\mathbf{p}_0^{\mathbf{x}}$  is the contribution of the initial condition  $\mathbf{x}_0$  to  $G(\mathbf{p}, t)$ . The dependence in  $t$  of  $G(\mathbf{p}, t)$  is implicit, encoded in the path  $(\mathbf{p}(t), \mathbf{q}(t))$  of integration.

The so-called semi-classical approximation (also called optimal fluctuation approximation, see [Dykman et al. 2008](#)) reduces the path integral Eq. (10) to its main contribution

$$G(\mathbf{p}, t) \approx \exp(-N_c S_0(\mathbf{p}, t)), \quad (12)$$

where  $S_0(\mathbf{p}, t)$  is the value of the action functional Eq. (11) integrated over an optimal path. We consider  $\Omega = N_c V_c$  where  $V_c$  is the typical volume of a T cell. As an estimation for  $V_c$ , we take the typical volume of a human mammalian cell in culture ([Bohil et al. 2006](#))  $V_c \simeq 2000 \mu\text{m}^3$ .  $N_c$  is now associated to the typical number of cells in a volume of blood  $\Omega$ . Using a WKB approximation, hence assuming  $N_c \gg 1$  ([Elgart and Kamenev 2004](#); [Assaf et al. 2010](#)), one can see that the optimal path is just a classical trajectory. Indeed substituting the WKB ansatz  $G(\mathbf{p}, t) = \exp(-N_c S(\mathbf{p}, t))$  into Eq. (9) one checks that the leading order of the expansion of  $S$  in powers of  $N_c^{-1}$

satisfies the Hamilton-Jacobi equation

$$\frac{\partial S(\mathbf{p}, t)}{\partial t} = -H\left(\mathbf{p}, \frac{\partial S(\mathbf{p}, t)}{\partial \mathbf{p}}\right), \quad (13)$$

where  $H$  denotes the associated classical Hamiltonian

$$\begin{aligned} H(\mathbf{p}, \mathbf{q}) = & \lambda(p_1 - 1) + d_T(1 - p_1)q_1 + (1 - \eta)(1 - \epsilon)k(p_3 - p_1p_4)q_1q_4 \\ & + \eta(1 - \epsilon)k(p_2 - p_1p_4)q_1q_4 + r\left(p_2^2 - p_2\right)q_2 + \frac{r}{2L_{\max}}\left(1 - p_2^2\right)q_2^2 \\ & + d_L(1 - p_2)q_2 + a_L(p_3 - p_2)q_2 + p_v(p_3p_4 - p_3)q_3 + \delta(1 - p_3)q_3 \\ & + c(1 - p_4)q_4 + \epsilon k(p_1 - p_1p_4)q_1q_4. \end{aligned} \quad (14)$$

In other words, denote by  $(q_i, p_i)$  the generalised coordinates corresponding to  $i$ -th cellular type. Note that the abbreviate action

$$S(\mathbf{p}, t) = \int \mathbf{p} d\mathbf{q}$$

along the classical trajectory differs from the Hamilton action by a constant (since the system is conservative and the time of integration is fixed). This means that to approximate  $G(\mathbf{p}, t)$  one can proceed to evaluate the abbreviate action along the solution of the boundary value problem defined by the Hamilton equations

$$\frac{dp_i}{dt} = -\frac{\partial H}{\partial q_i}, \quad \frac{dq_i}{dt} = \frac{\partial H}{\partial p_i}, \quad (15)$$

with boundary conditions  $q_i(0) = x_i(0)$  and  $p_i(t) = p_i$ , where  $p_i$  is the momentum corresponding to species  $i$ , see [Elgart and Kamenev \(2004\)](#) for further details. Details on the concrete computations are give in “Appendix 1”. Note that by taking  $p_i(t) = 1$  for all  $i$  in Eq. (17), the mean-field Eqs. (2)–(5) are recovered. Furthermore, since  $H(\mathbf{q}, \mathbf{p} = \mathbf{1}) = 0$  [see Eq. (14)],  $S(\mathbf{p} = \mathbf{1}, t) = 0$  holds and therefore the normalisation condition  $G(\mathbf{p} = \mathbf{1}, t) = 1$  is satisfied.

Equation (10) shows that rare events, which, for the purpose of this paper, are those whose frequency decays exponentially with system size, of which extinctions are a particular case, are described by classical trajectories accumulating around the optimal one ([Dykman et al. 1994](#)). For this reason, the associated path integral can be computed by means of a saddle point method near the optimal trajectory which maximises the action functional Eq. (11), which is found by solving the associated Hamilton equations with the appropriate boundary conditions. To analyse extinction events, these boundary conditions are  $(q_i(-\infty), p_i(-\infty)) = (y_i, 1)$ , where  $y_i$  are the coordinates of the positive stable equilibrium of the mean-field dynamics (see Sect. 2), and  $(q_i(\infty), p_i(\infty)) = (0, p_i^*)$  (see Fig. 5). Using several versions of the WKB method and the optimal fluctuation approach, it has been shown that the average waiting time for rare events, including extinction, is given by [Dykman et al. \(1994\)](#), [Elgart and Kamenev \(2004\)](#), [Kamenev and Meerson \(2008\)](#), [Dykman et al. \(2008\)](#),

Assaf and Meerson (2010) and Assaf et al. (2010):

$$\tau_E = AN_c^B \exp(N_c C), \quad (16)$$

where  $C$  is such that  $S_0 = N_c C$ , where  $S_0$  is the action calculated over the heteroclinic trajectory connecting two fixed points of the Hamilton equations (17): the mean-field positive equilibrium fixed point,  $(q_i(-\infty), p_i(-\infty)) = (y_i, 1)$ , which is also a fixed point of the Hamiltonian system Eq. (17), and the extinction fixed point  $(q_i(\infty), p_i(\infty)) = (0, p_i^*)$ . As time goes to infinity, the trajectories approach the  $H(p, q) = 0$  energy level. The action functional vanishes on  $p_i = 1$  and on  $q_2 = q_3 = q_4 = 0$ . However, it is positive on the heteroclinic connection between the metastable state and the stochastic extinction state, which is of the form  $q_2 = q_3 = q_4 = 0, 0 < p_i < 1$ . For higher-dimensional systems, the numerical computation of this heteroclinic connection usually requires the use of numerical methods. This numerical methodology is aided by the fact that, by exploiting the multiplicity of time scales present in our system, i.e. by using a quasi-steady state approximation (QSSA), we can reduce the dimensionality of the system Eq. (15). The quasi-steady state reduction of the equations of motion is explained in detail in “Appendix 1”, where we show that a hierarchy of time scales is present in our system [see Eq. (23)], “Appendix 1” that allows to reduce the Hamiltonian system from 4 degrees of freedom to 1 (strong QSSA) or 2 (weak QSSA). Such reduction renders the problem of computing numerically heteroclinic connections more tractable.

The heteroclinic connection is crucial to estimate  $C$  in Eq. (16). The computation of the heteroclinic connection in the 1 degree of freedom (1-dof) Hamiltonian is straightforward, however with 2-dof is not trivial at all. In “Appendix 1” we explain the different techniques we use to compute the heteroclinic connection for the 2-dof case.

To fully determine  $\tau_E$  we need to get  $A$  and  $B$ . In order to obtain these parameters in the expression (16), we perform a numerical fit of  $A$  and  $B$  using numerical results obtained by means of multi-scale stochastic simulations (Cao et al. 2005), in which  $\tau_E$  is computed for different values of  $\Omega$ . These simulation results, together with Eq. (16) and the corresponding value of  $C$ , are used to fit the values of  $A$  and  $B$ . The technical details regarding this procedure are included in “Appendix 1”.

## 4 Results

In this section, we analyse the feasibility of the combination HAART-LICST in terms of the study of how the average extinction time of the infection changes as the activation rate of the latently infected cells varies, and some possible side effects of such combination therapy. The accuracy of our asymptotic and numerical results, obtained by means of the methodology explained in Sect. 3, are checked by comparing to simulation results obtained by using a hybrid multi-scale Monte-Carlo simulation algorithm (Cao et al. 2005).

#### 4.1 Effect of LICST on the average extinction time

We consider the extinction dynamics of the infection in the subcritical regime, i.e.  $a_L < a_L^*$  (see Eq. 6). Our aim is to analyse the effect of combined HAART-LICST on the average extinction time. Our basic assumption is that LICST upregulates the latently infected cell activation rate. Therefore we study how the infection average extinction time, given by Eq. (16), varies as the value of  $a_L$  is changed.

In order to proceed further, we first need to assess the accuracy of our asymptotic approximations (see Sect. 3). Numerical computation of the average extinction time for our stochastic infection model in terms of the regular stochastic simulation algorithm (Gillespie 1976) requires a huge amount of computational time, particularly for values of  $a_L$  close to their physiological estimates (Rong and Perelson 2009). In order to reduce the computation time, we use a multi-scale hybrid stochastic simulation method proposed by Cao et al. (2005), which takes advantage of the separation of time scales in our system to improve the numerical efficiency of the method. The Gillespie simulations suggest that the reactions corresponding to production and degradation of the virus ( $T^* \rightarrow T^* + V$  and  $V \rightarrow \emptyset$ ) are 500 times more common than the reactions that change the number of latently or productively infected cells, therefore, we are in the perfect scenario to use this method. In Fig 2, we compare the average extinction time obtained by three different methods: Gillespie SSA, multi-scale hybrid SSA, and our semi-classical approximation using the strong QSSA (see “Appendix 1”). We carry out this comparison in a restricted range of values of  $a_L$  where the Gillespie algorithm runs in a reasonable computational time. We observe rather good agreement between all three methods, which gives us confidence of the suitability of both the multi-scale simulation method and our asymptotic approximation, and justifies the use of these methods to reach a wider range of values of  $a_L$ . Discrepancies between the semi-classical QSSA approximation and the numerical results are observed for larger values of  $a_L$  as  $a_L \rightarrow a_L^*$ , i.e. the critical value of  $a_L$  above which the mean-field positive equilibrium ceases to exist. In spite of this discrepancy, our semi-classical QSSA approximation appears to be rather accurate, in particular for smaller values of  $a_L$ , close to its physiological estimate, which is precisely the range of values of  $a_L$  for which the average waiting time is larger, and, therefore, where we expect both stochastic simulation algorithms to perform poorly.

Apart from checking the accuracy of our semi-classical approximation, Fig. 2b shows an interesting result: the average extinction time,  $\tau_E$ , decreases as the value of  $a_L$  increases, thus suggesting that the LICST therapy could be effective in reducing the time to eradication of the HIV infection. These results are confirmed when  $S_0$  is computed over a wider range of values of  $a_L$ . Figure 3a shows how, as the value of  $a_L$  increases,  $S_0$  decreases in such a way as to induce a very dramatic decrease in  $\tau_E$  of many orders of magnitude (recall that  $S_0 \sim \log(\tau_E)$ ). In fact, looking at the results of Fig. 2b, we conclude that the average extinction time of the infection could be reduced to  $\tau_E \approx 1000$  days, provided that the drugs used are efficient enough to drive the value of  $a_L$  close to its critical value. Incidentally, Fig. 3a shows the results for the

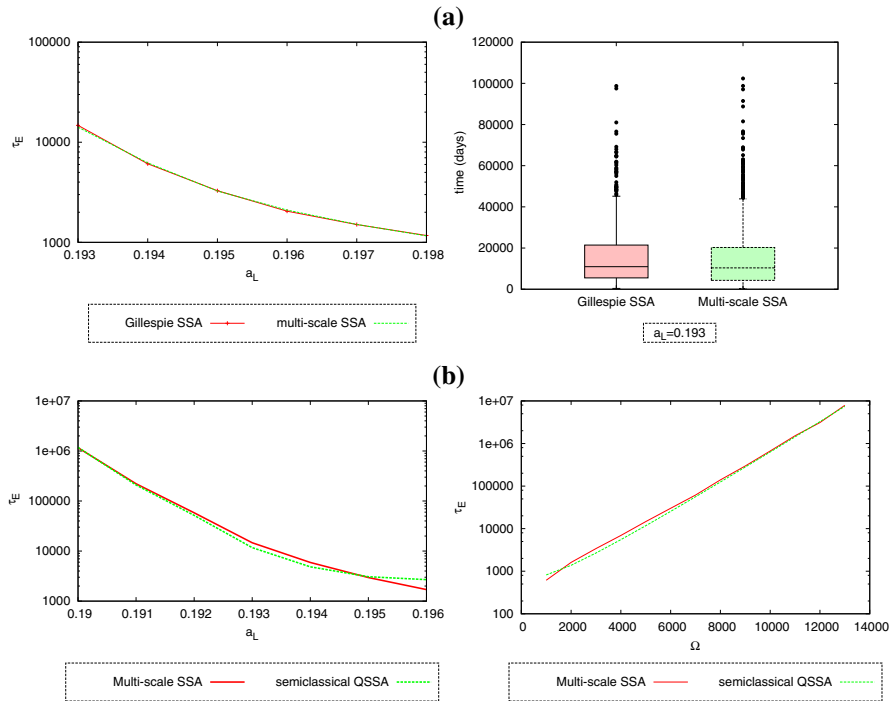


**Fig. 2** Series of plots showing the average extinction time of the HIV-1 infection as a function of the activation rate of the latently infected cells,  $a_L$ . **a** Comparison between the results obtained using the standard Gillespie SSA (Gillespie 1976) and the multi-scale hybrid SSA (Cao et al. 2005) (left). Average of extinction time over 1000 simulations in both cases for different values of  $a_L$  (right). Boxplot of SSA and multi-scale SSA for  $a_L = 0.193$  computed with 1000 simulations in both cases. **b** (Left) Comparison between the asymptotic results obtained using the Strong QSSA (see “Appendix 1”) and numerical simulations obtained by means multi-scale hybrid SSA (Cao et al. 2005). In the latter case, average has been taken over 1000 simulations. The discrepancy observed between the semi-classical QSSA approximation and the numerical results for larger values of  $a_L$  arises because we are approaching  $a_L^*$ , i.e. the critical value of  $a_L$  above which the mean-field positive equilibrium ceases to exist. (Right) Comparison of the value of  $\tau_E$  obtained using the semiclassical approximation and multi-scale SSA as a function of the system size,  $\Omega$ , for a fixed value of  $a_L = 0.193$ , as it was expected, the approximation works better for a larger values of  $\Omega$ . All remaining parameter values are as shown in Table 2

optimal value of the action functional computed by integration over the heteroclinic connection between the mean-field positive equilibrium and the stochastic extinction fixed point,  $S_0$ , for both the strong QSSA and the weak QSSA (see “Appendix 1”). These results show excellent agreement between both approximations, thus suggesting that the Strong QSSA, i.e. the least numerically demanding, can be used without a significant loss of accuracy. Figure 3b shows results for the average extinction time,  $\tau_E$ , calculated using the Strong QSSA over an interval of values of the activation rate,  $a_L$ , ranging from its physiological value  $a_L = a_L^s = 0.1$  (see Table 2) to values close to its critical value  $a_L \rightarrow a_L^*$  (see Table 2). We observe that  $\tau_E$  decreases over many orders of magnitude when  $a_L$  varies within this interval.



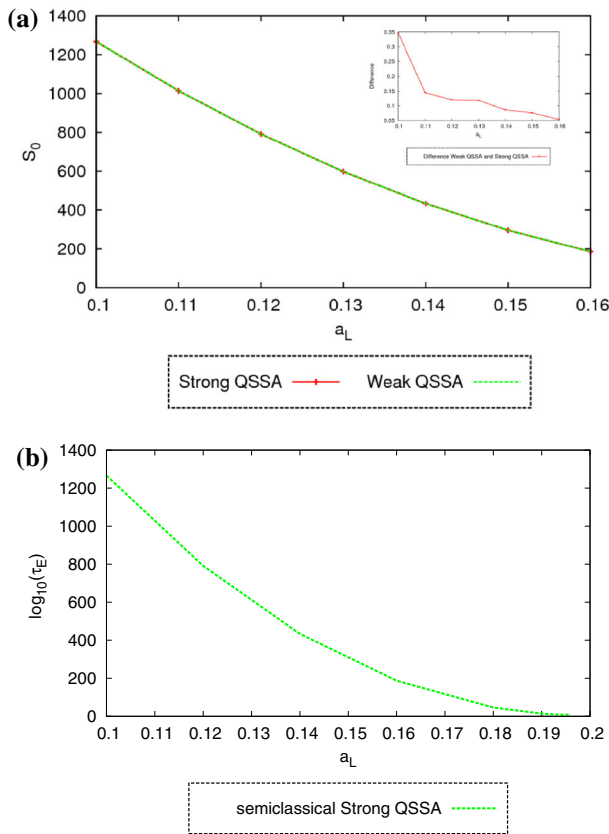


**Fig. 3** **a** Plot showing how the value of the action integrated along the heteroclinic connection,  $S_0$ , varies as  $a_L$  changes. We have computed  $S_0$  with both the Strong QSSA (red line) and the Weak QSSA (green line). The inset shows the difference between the Strong QSSA estimate and the Weak QSSA estimate. **b** Plot showing the change of the average extinction time,  $\tau_E$ , according to the Strong QSSA, as  $a_L$  varies. All remaining parameter values are taken from Table 2

## 4.2 Side effects of LICST: viral blips

The analysis of the mean-field dynamics shows that an increment of  $a_L$  reduces the viral load associated to the metastable state (i.e. the mean-field positive equilibrium). However, in order to assess the viability of LICST, we must check the transient effects of LICST, as the upregulation of the activation of the latently infected cell compartment leads to a transient increase in the viral load (Rong and Perelson 2009). In this section, we study this transient behaviour to assess whether the viral load increases to threatening levels upon stimulation of latently infected cell activation, or if, on the contrary, it remains within tolerable levels.

To study this issue, we have performed stochastic simulations of the stochastic infection model which we have set up as follows. We fix an initial condition  $(y_1, y_2, y_3, y_4) \equiv (T_0, L_0, T_0^*, V_0)$ , where  $T_0$ ,  $L_0$ ,  $T_0^*$  and  $V_0$  are the mean-field steady

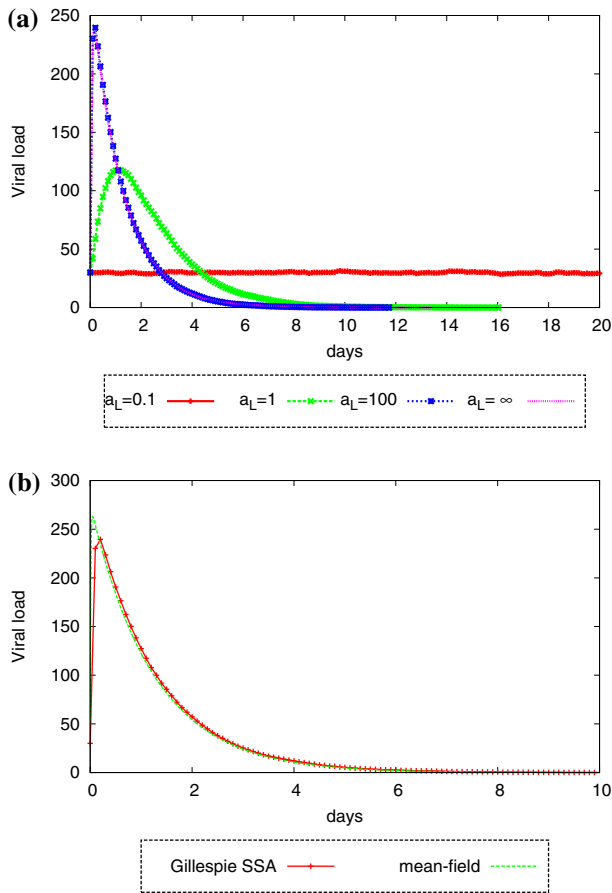


**Fig. 4** Series of plots showing the response of the viral load as  $a_L$  is increased to  $a_L > a_L^S = 0.1$ . Plot **a** shows stochastic simulations of the viral dynamics for different values of  $a_L$ . For reference, we also show simulation results where  $a_L$  is kept constant at  $a_L = a_L^S$ . Plot **b** shows the comparison between a stochastic simulations and the mean-field behaviour of the viral dynamics for  $a_L = 100$ . Note that we have used unphysiologically large values of  $a_L$  to illustrate that the peak reached by the viral load upon LICST. All remaining parameter values are taken from Table 2

state values of the number of uninfected T cells, latently and active infected cells, and viral load, respectively. We consider the steady state associated to the physiological estimate of  $a_L = a_L^S = 0.1$ . We then increase  $a_L$  to a value  $a_L > a_L^S$  and let the system to evolve.

Figure 4a (left) shows our simulation results for different values of  $a_L > a_L^S$ . Our results, in agreement with previous studies of similar situations (Rong and Perelson 2009), we observe that upon application of LICST (i.e. after increasing the value of  $a_L$ ), there is a transient increase of the viral load, which, depending on the value of  $a_L$ , can be elevated beyond the detection threshold of standard assays (50 mRNA/ml). As time progresses, the viral load peaks at a maximum value and starts decreasing. We observe that the peak value reached by the viral load grows as  $a_L$  increases. However,

it saturates for large values of  $a_L$ . By contrast, the duration of the blip is a decreasing function of  $a_L$ . This behaviour is well captured by the mean-field limit (see Fig. 4b).

## 5 Conclusions

We have presented and analysed a stochastic model of HIV-1 dynamics under the combined action of highly active anti-retroviral therapy and latently infected cell stimulation therapy with the aim of analysing the effectiveness and feasibility of this combination therapy. In order to carry out our quantitative evaluation, we study how the average extinction time is affected as the rate of activation of latently infected cells is varied. To this end, we have employed asymptotic techniques in combination with advanced numerical methods. The accuracy of the asymptotic results has been evaluated by comparing with Monte Carlo stochastic simulations algorithms.

Our asymptotic analysis, based on the formulation of an optimal fluctuation theory based on a semi-classical approximation (Assaf and Meerson 2010; Kubo et al. 1973; Elgart and Kameney 2004) for the PDE of the probability generating function,  $G(p, t)$ , has revealed that our system exhibits a hierarchical multi-scale nature, whereby each variable has a different time scale. This property has been exploited to reduce the dimensionality of the problem: we have adapted the technique developed in Alarcón (2014) and de la Cruz et al. (2014) to perform a time-scale analysis of the Hamilton equations associated to the optimal fluctuation path to formulate two different QSS approximations. Similarly, separation of time-scales have also been used to justify the use of a multi-scale hybrid stochastic algorithm (Cao et al. 2005) in order to validate our asymptotic results.

Using this methodology, we have analysed how the average extinction time varies under a form of therapy which involves the change (increase) of the rate of activation of the latently infected. We have determined that the administration of such therapy reduces the average extinction time,  $\tau_E$ , by many orders of magnitude when  $a_L$  is increased with respect to its physiological estimate,  $a_L^S$ , shown in Table 2. We have shown that, provided the drugs are powerful enough to drive the value of  $a_L$  close to its critical value,  $a_L^*$  (see Sect. 2),  $\tau_E$  can be reduced to  $\tau_E \approx 1000$  days.

We have also analysed the side effects of this therapy, by looking at the response of the viral load upon change of the value of the activation rate,  $a_L$ . We have shown that, although a transient increase in viral load, the peak value reached by viral load is bounded (of the order of 250 copies/ml) and well below the life-threatening levels observed in an untreated (no HAART) patient (of the order of  $10^5$  copies/ml (Rong and Perelson 2009)).

In view of this results, we conclude that this therapy appears to be both effective (in terms of the reduction of the average extinction time from longer than the patient life expectancy to 2–3 years) and feasible (in terms of the bounded peak reached by the viral load upon its administration). However, a few caveats are in order. First, following (Chomont et al. 2009; Rong and Perelson 2009), we have considered that the size of the latent compartment is under homeostatic control by means of a size-dependent birth rate of the latently infected cells (see Sect. 2). From the point of view of our model, this implies that the mean-field positive equilibrium is more stable than

it would be if we did not consider such homeostatic control. In quantitative terms this means that the average extinction time (both with and without LICST) would be considerably smaller than the ones reported here. Although assuming no homeostatic control (Siliciano et al. 2003) of the latently infected population would not alter our qualitative results (i.e. increasing  $a_L$  would still lead to a decrease in  $\tau_E$ ), the analysis should be repeated to obtain accurate quantitative estimates. In any case, our current quantitative results would still be upper bounds. Furthermore, our LICST model is not properly calibrated in the sense that we do not have quantitative information available about how much of an increase in  $a_L$  current latent cell-stimulating drugs can induce. More accurate models and experimental information regarding the effect of current drugs on latently infected cells is needed before such calibrated model is possible. We left for future work the study of the effect of the therapy modeled as a non-stationary impulse, i.e. either with a periodic function, or a more accurate model including how the levels of histone deacetylases and other chromatic modifiers change the activation of the latently infected cells (Trono et al. 2010).

From the theoretical point of view, we have not been able to fully determine the value of  $\tau_E$  from our asymptotic method: the semi-classical approximation, Eq. (16), provides the exponential scaling but it does not give any information regarding the prefactor, i.e. the parameters  $A$  and  $B$ , which need to be fitted to numerical simulations. A more accurate asymptotic theory able to provide the prefactor should be developed based on WKB methods (Assaf et al. 2010) or matching-asymptotic expansions (Ward 1998), or on a better understanding of the associated Stokes phenomenon. All these issues are beyond the scope of the current work and left for future research. Despite these issues, we expect that the methodological aspects developed in this paper are useful to and find their way into the study of the stochastic aspects of other similar systems involving infection dynamics and the evaluation of the effectiveness of newly developed treatments.

**Acknowledgments** D.S.T. and T.A. acknowledge the Spanish Ministry for Science and Innovation (MICINN) for funding under Grant MTM2011-29342 and Generalitat de Catalunya for financial support under Grant 2014SGR1307. A.V. has been supported by Grants MTM2010-16425 and MTM2013-41168-P (Spain) and 2014 SGR 1145 (Catalonia). This work was done during the stay of A.V. at the Centre de Recerca Matemàtica (CRM, Catalunya), he warmly thanks the CRM for the facilities and support. The computing facilities of the UB Dynamical Systems Group have been largely used, the authors thank J. Timoneda for the technical support. T.A. acknowledges support from the Ministry of Economy and Competitiveness (MINECO) for funding awarded to the Barcelona Graduate School of Mathematics under the “María de Maeztu” programme, Grant Number MDM-2014-0445.

## Appendix 1: Time-scale analysis: weak and strong quasi-steady state approximations

In this appendix, we proceed to formulate a quasi-steady approximation, that allows us to simplify the equations of motion of the Hamiltonian (14), which are of the form

$$\begin{aligned} \frac{dp_1}{dt} = & d_T(p_1 - 1) + (1 - \eta)(1 - \epsilon)k(p_1 p_4 - p_3)q_4 + \eta(1 - \epsilon)k(p_1 p_4 - p_2)q_4 \\ & + \epsilon k(p_1 p_4 - p_1)q_4, \end{aligned}$$

$$\begin{aligned}
\frac{dp_2}{dt} &= r(p_2 - p_2^2) + \frac{r}{L_{max}}(p_2^2 - 1)q_2 + d_L(p_2 - 1) + a_L(p_2 - p_3), \\
\frac{dp_3}{dt} &= p_v(p_3 - p_3p_4) + \delta(p_3 - 1), \\
\frac{dp_4}{dt} &= (1 - \eta)(1 - \epsilon)k(p_1p_4 - p_3)q_1 + \eta(1 - \epsilon)k(p_1p_4 - p_2)q_1 + c(p_4 - 1) \\
&\quad + \epsilon k(p_1p_4 - p_1)q_1, \\
\frac{dq_1}{dt} &= \lambda - d_Tq_1 - (1 - \epsilon)kp_4q_1q_4 + \epsilon k(1 - p_4)q_1q_4, \\
\frac{dq_2}{dt} &= \eta(1 - \epsilon)kq_1q_4 + r(2p_2 - 1)q_2 - \frac{r}{L_{max}}p_2q_2^2 - d_Lq_2 - a_Lq_2, \\
\frac{dq_3}{dt} &= (1 - \eta)(1 - \epsilon)kq_1q_4 + a_Lq_2 + p_v(p_4 - 1)q_3 - \delta q_3, \\
\frac{dq_4}{dt} &= -kp_1q_1q_4 + p_vp_3q_3 - cq_4.
\end{aligned} \tag{17}$$

We proceed by re-scaling our variables in such a way to make explicit the separation of time scales and simplify the model according to the quasi-steady state approximation. For clarity, we perform this analysis in two steps. We start by defining the following set of re-scaled (dimensionless) quantities:

$$\begin{aligned}
\bar{q}_1 &= \frac{q_1}{T_0}, \quad \bar{q}_2 = \frac{q_2}{L_0}, \\
\bar{q}_3 &= \frac{q_3}{T_0^*}, \quad \bar{q}_4 = \frac{q_4}{V_0}, \\
s &= kV_0t.
\end{aligned} \tag{18}$$

The momenta  $p_i$  are not re-scaled. In this re-scaled variables, the re-scaled Hamiltonian,  $H_\kappa(\mathbf{p}, \bar{\mathbf{q}})$ , is defined by Alarcón (2014) and de la Cruz et al. (2014):

$$H(\mathbf{p}, \mathbf{q}) = kT_0V_0H_\kappa(\mathbf{p}, \bar{\mathbf{q}}), \tag{19}$$

where  $H_\kappa(\mathbf{p}, \mathbf{q})$  is given by:

$$\begin{aligned}
H_\kappa(\mathbf{p}, \mathbf{q}) &= \kappa_1(p_1 - 1) + \kappa_2(1 - p_1)q_1 + (1 - \eta)(1 - \epsilon)(p_3 - p_1p_4)q_1q_4 \\
&\quad + \eta(1 - \epsilon)(p_2 - p_1p_4)q_1q_4 + \kappa_3\left(p_2^2 - p_2\right)q_2 + \kappa_3\frac{L_0}{2L_{max}}\left(1 - p_2^2\right)q_2^2 \\
&\quad + \kappa_4(1 - p_2)q_2 + \kappa_5(p_3 - p_2)q_2 + \kappa_6(p_3p_4 - p_3)q_3 + \kappa_7(1 - p_3)q_3 \\
&\quad + \kappa_8(1 - p_4)q_4 + \epsilon(p_1 - p_1p_4)q_1q_4.
\end{aligned} \tag{20}$$

For simplicity of the notation, we have dropped the bars of the re-scaled variables  $\bar{q}_i$ . The parameters  $\kappa_i$  are defined in Table 3.

**Table 3** Re-scaled parameters associated to the re-scaling of variables Eq. (18) and to the re-scaled Hamiltonian Eq. (20)

| Parameter                               | Order of magnitude |
|---|--------------------|
| $\kappa_1 = \frac{\lambda}{kT_0V_0}$    | $O(10^5)$          |
| $\kappa_2 = \frac{dT}{kV_0}$            | $O(10^5)$          |
| $\kappa_3 = \frac{rL_0}{kV_0T_0}$       | $O(10^0)$          |
| $\kappa_4 = \frac{d_L L_0}{kV_0T_0}$    | $O(10^{-2})$       |
| $\kappa_5 = \frac{a_L L_0}{kV_0T_0}$    | $O(10^0)$          |
| $\kappa_6 = \frac{p_v T_0^*}{kV_0T_0}$  | $O(10^3)$          |
| $\kappa_7 = \frac{\delta T_0}{kV_0T_0}$ | $O(10^0)$          |
| $\kappa_8 = \frac{c}{kT_0}$             | $O(10^3)$          |

The Hamilton equations for the re-scaled variables read as follows:

$$\begin{aligned}
 \frac{dq_1}{ds} &= \frac{\partial H_\kappa}{\partial p_1}, & \frac{dp_1}{ds} &= -\frac{\partial H_\kappa}{\partial q_1}, \\
 \frac{L_0}{T_0} \frac{dq_2}{ds} &= \frac{\partial H_\kappa}{\partial p_2}, & \frac{L_0}{T_0} \frac{dp_2}{ds} &= -\frac{\partial H_\kappa}{\partial q_2}, \\
 \frac{T_0^*}{T_0} \frac{dq_3}{ds} &= \frac{\partial H_\kappa}{\partial p_3}, & \frac{T_0^*}{T_0} \frac{dp_3}{ds} &= -\frac{\partial H_\kappa}{\partial q_3}, \\
 \frac{V_0}{T_0} \frac{dq_4}{ds} &= \frac{\partial H_\kappa}{\partial p_4}, & \frac{V_0}{T_0} \frac{dp_4}{ds} &= -\frac{\partial H_\kappa}{\partial q_4}.
 \end{aligned} \tag{21}$$

In order to proceed further with our time-scale analysis, we note that the re-scaled equations associated to  $q_1$  and  $q_4$  are dominated by the terms in  $\kappa_1$  and  $\kappa_2$ , which, according to Table 3, are  $O(10^5)$ , and  $\kappa_6$  and  $\kappa_8$ , which are  $O(10^3)$ , respectively. On the contrary, the dominant terms in the equations for  $q_2$  and  $q_3$  are  $O(1)$ . In view of this, we re-scale the dimensionless time  $s$  as:

$$T = \kappa_1 s. \tag{22}$$

From Hamiltonian (20) already in rescaled variables (18), we derive two approximations of the system of equations using the slow-fast time-scales variables. In the new time  $T$  and denoting  $' = d/dT$ , the equations of motions are

$$\begin{aligned}
 q_1' &= \frac{1}{\kappa_1} \frac{\partial H_\kappa}{\partial p_1}, & p_1' &= \frac{1}{\kappa_1} \frac{\partial H_\kappa}{\partial q_1}, \\
 \epsilon_1 q_2' &= \frac{\partial H_\kappa}{\partial p_2}, & \epsilon_1 p_2' &= \frac{\partial H_\kappa}{\partial q_2}, \\
 \epsilon_2 q_3' &= \frac{\partial H_\kappa}{\partial p_3}, & \epsilon_2 p_3' &= \frac{\partial H_\kappa}{\partial q_3},
 \end{aligned} \tag{23}$$

$$\epsilon_3 q'_4 = \frac{1}{\kappa_6} \frac{\partial H_\kappa}{\partial p_4}, \quad \epsilon_3 p'_4 = \frac{1}{\kappa_6} \frac{\partial H_\kappa}{\partial q_4},$$

where  $\epsilon_1 = \kappa_1 \frac{L_0}{T_0} = O(10^{-1})$ ,  $\epsilon_2 = \kappa_1 \frac{T_0^*}{T_0} = O(10^{-2})$ , and  $\epsilon_3 = \frac{\kappa_1}{\kappa_6} \frac{L_0}{T_0} = O(10^{-3})$ , according to the values in Table 3. The right hand side of the previous system of equations is  $O(1)$ .

First we assume that the pair  $(q_1, p_1)$ , associated to the uninfected T cells, is such that  $(q_1, p_1) \approx (T_0, 1)$ . This is somehow justified due to the rather huge number of uninfected T cells. A similar approximation has been used in prior stochastic models of the HIV-1 infection (Conway and Coombs 2011). Accordingly, we assume  $q'_1 \approx 0$  and  $p'_1 \approx 0$ , and the system becomes a 3-dof Hamiltonian system.

We refer as the *strong* QSSA to the 1-dof Hamiltonian system obtained assuming  $\epsilon_2 q'_3 = \epsilon_2 p'_3 \simeq 0$  and  $\epsilon_3 q'_4 = \epsilon_3 p'_4 \simeq 0$  [i.e. we apply QSS conditions to the pairs  $(p_3, q_3)$  and  $(p_4, q_4)$ ]. The corresponding equations are

$$\begin{aligned} p'_2 &= \frac{1}{\epsilon_1} \left( -\kappa_3 (p_2^2 - p_2) - \kappa_3 \frac{L_0}{L_{max}} (1 - p_2^2) q_2 - \kappa_4 (1 - p_2) - \kappa_5 (p_3 - p_2) \right), \\ q'_2 &= \frac{1}{\epsilon_1} \left( \eta \tilde{\epsilon} q_1 q_4 + \kappa_3 q_2 (2p_2^2 - 1) - \kappa_3 \frac{L_0}{L_{max}} p_2 q_2^2 - \kappa_4 q_2 - \kappa_5 q_2 \right), \end{aligned} \quad (24)$$

where  $\tilde{\epsilon} = 1 - \epsilon$ ,  $\tilde{\eta} = 1 - \eta$ ,  $p_1 = q_1 = 1$ ,

$$\begin{aligned} p_3 &= \frac{\Delta \pm \sqrt{\Delta^2 - 4\kappa_7 \kappa_6 A}}{2\kappa_6 A}, \quad q_3 = \frac{-\kappa_5 q_2}{\tilde{\eta} \tilde{\epsilon} q_1 D p_3 + \kappa_6 (A p_3 + B p_2 + C) - \kappa_7 q_3}, \\ p_4 &= \frac{-\tilde{\eta} \tilde{\epsilon} q_1 p_3 - \tilde{\eta} \tilde{\epsilon} p_2 q_1 - \kappa_8 - \epsilon p_1 q_1}{\Gamma}, \quad q_4 = \frac{\kappa_6 p_3 q_3}{p_1 q_1 + \kappa_8}, \end{aligned} \quad (25)$$

and

$$\begin{aligned} A &= \frac{-(1 - \eta)(1 - \epsilon)q_1}{\Gamma}, \quad B = \frac{-\eta(1 - \epsilon)p_2 q_1}{\Gamma}, \quad C = \frac{-\kappa_8 - \epsilon p_1 q_1}{\Gamma}, \\ D &= \frac{\kappa_6}{p_1 q_1 + \kappa_8}, \\ \Delta &= \kappa_6 - \kappa_7 - C \kappa_6 - B \kappa_6 p_2, \quad \Gamma = -(1 - \eta)(1 - \epsilon)q_1 p_1 - \eta(1 - \epsilon)p_1 q_1 \\ &\quad - \kappa_8 - \epsilon p_1 q_1. \end{aligned}$$

We can discard the positive branch of  $p_3$  by continuity. A phase portrait of the strong QSSA is shown in Fig. 5.

We refer as the *weak* QSSA to the 2-dof approximation obtained by just assuming  $\epsilon_3 q'_4 = \epsilon_3 p'_4 \simeq 0$  [i.e. applying QSS conditions to the pair  $(q_4, p_4)$ ]. The differential equations are

$$p'_2 = \frac{1}{\epsilon_1} \left( -\kappa_3 (p_2^2 - p_2) - \kappa_3 \frac{L_0}{L_{max}} (1 - p_2^2) q_2 - \kappa_4 (1 - p_2) - \kappa_5 (p_3 - p_2) \right),$$

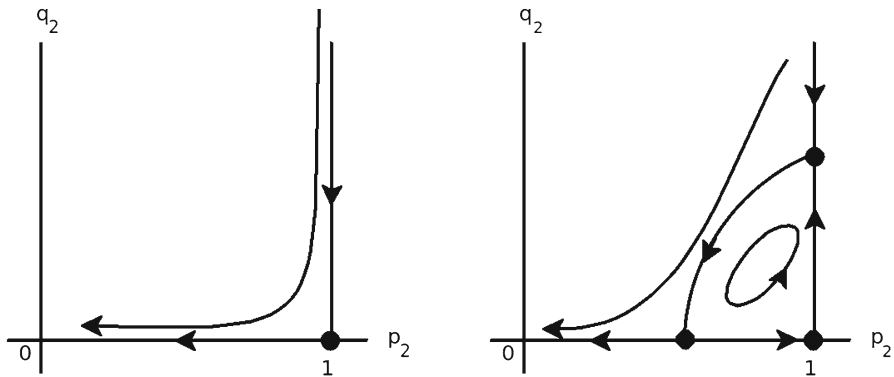


**Fig. 5** Phase diagram of the reduced system of equations of motion associated to the Strong QSS approximation, Eq. (24), in the supercritical case (*left*) and the subcritical case (*right*). The subcritical case corresponds to the case where the mean-field dynamics exhibits a stable positive equilibrium. In this case, there exists a non-trivial, zero-energy heteroclinic trajectory connecting the mean-field positive equilibrium and the stochastic extinction fixed point

$$\begin{aligned}
 q_2' &= \frac{1}{\epsilon_1} \left( \tilde{\eta} \tilde{\epsilon} q_1 q_4 + \kappa_3 q_2 (2p_2^2 - 1) - \kappa_3 \frac{L_0}{L_{max}} p_2 q_2^2 - \kappa_4 q_2 - \kappa_5 q_2 \right), \\
 p_3' &= \frac{1}{\epsilon_2} (-\kappa_6 (p_3 p_4 - p_3) - \kappa_7 (1 - p_3)), \\
 q_3' &= \frac{1}{\epsilon_2} (\tilde{\eta} \tilde{\epsilon} q_1 q_4 + \kappa_5 q_2 + \kappa_6 (p_4 - 1) q_3 - \kappa_7 q_3),
 \end{aligned} \tag{26}$$

where, as before,  $\tilde{\epsilon} = 1 - \epsilon$ ,  $\tilde{\eta} = 1 - \eta$ ,  $p_1 = q_1 = 1$  and  $p_3$  and  $p_4$  are given by (25).

## Appendix 2: Computation of the heteroclinic trajectory in the weak QSSA

In Sect. 3.1.1, we have discussed how the average extinction time is estimated within the semi-classical approximation (or the optimal fluctuation theory) by computing the value of the action functional by integration over the optimal path,  $S_0$ , which corresponds to the heteroclinic connection between the mean-field positive equilibrium and the stochastic extinction fixed point. The corresponding estimates of  $S_0$  are obtained after performing either a one-step (weak) or a two-step (strong) quasi-stationary approximation of the classical equations of motion, see “Appendix 1”, and computing the integral of the classical action  $S$  along the only non-trivial path connecting the metastable state and the stochastic extinction of the system. Looking at the phase space of the mean field system, one realizes that this non-trivial path is given by the heteroclinic trajectory  $\gamma(t)$  from the hyperbolic fixed point  $\mathbf{p}_1$  (with  $p_i = 1$  and  $x_i > 0$ ) and the fixed point  $\mathbf{x}_0$  located on  $x_i = 0$  with  $0 < p_i < 1$  (here  $i = 2$  for the strong QSS approximation and  $i = 1, 2$  for the weak QSS case).

It is a simple exercise to obtain an expression of the heteroclinic connection in the strong QSS approximation, since, under this approximation, the system is reduced to one degree of freedom, and, therefore, the heteroclinic trajectory is simply determined



by conservation of energy. However, the computation of  $\gamma(t)$  requires numerical techniques for the weak QSSA case since one has to deal with a 2 degrees of freedom (2-dof) Hamiltonian system. Moreover, the weak QSSA reduction exhibits a slow-fast structure, hence one has to deal with two quite different time-scalings when performing the numerics. We should note that all the computations have been performed using multiprecision arithmetics (around 100 digits where enough for most of the  $a_L$  values considered) and the codes have been implemented in PARI/GP (Batut et al. 1995).

Let us consider, from now on, the 2-dof Hamiltonian case whose related equations of motion, given by (26), are expressed in the coordinates  $x_2, x_3, p_2, p_3$ . The hyperbolic-hyperbolic fixed point  $\mathbf{p}_1$  has a 2-dimensional stable and a 2-dimensional unstable invariant manifold, to be denoted  $W^s(\mathbf{p}_1)$  and  $W^u(\mathbf{p}_1)$  respectively. Similarly,  $W^{s/u}(\mathbf{x}_0)$  will denote the 2-dimensional stable/unstable manifold associated to the fixed hyperbolic-hyperbolic point  $\mathbf{x}_0$ . The heteroclinic connection  $\gamma(t)$  corresponds to the intersection  $W^u(\mathbf{p}_1) \cap W^s(\mathbf{x}_0)$ .

To compute  $W^u(\mathbf{p}_1)$  (and also  $W^s(\mathbf{x}_0)$ ) we use the so-called parametrization method (Cabr   et al. 2005). Basically the idea is the following. We represent the local invariant manifold around  $\mathbf{p}_1$  as a vector series  $K(s_1, s_2)$ , being  $K : \mathbb{R}^2 \rightarrow \mathbb{R}^4$ . That is, a point  $X = (x_2, x_3, p_2, p_3) \in \mathbb{R}^4$  will be considered to be on  $W^u(\mathbf{p}_1)$  if  $X = K(s_1, s_2) = \sum_{i,j \geq 0} a_{i,j} s_1^i s_2^j$ . The coefficients  $a_{i,j} \in \mathbb{R}$  can be order by order computed by imposing the so-called invariance condition. This condition requires that the dynamics within the invariant manifold, expressed in the  $s_1, s_2$  coordinates, must be conjugated to the linear dynamics around the hyperbolic-hyperbolic point. Denote by  $\lambda_1, \lambda_2 > 0$  (resp.  $< 0$ ) the real eigenvalues associated to  $\mathbf{p}_1$  (resp. to  $\mathbf{x}_0$ , below we denote by  $K^{p_1}$  and  $K^{x_0}$  the corresponding parametrizations). Then, the linear dynamics is  $\dot{s}_1 = \lambda_1 s_1, \dot{s}_2 = \lambda_2 s_2$ . If  $\dot{X} = f(X)$  refers to the differential equations (26), then the invariance condition requires

$$\frac{\partial K}{\partial s_v}(s_1, s_2) \lambda_v s_v = f(K(s_1, s_2)), \quad v = 1, \dots, 2.$$

By imposing this equality order by order, being  $k = i + j \geq 1$  the total order, one gets a sequence of linear systems for the coefficients  $a_{i,j}, k > 1$  (for  $k = 0$  one gets the fixed point condition, and for  $k = 1$  the eigenvectors system). See Sim   (1990) for further details on this procedure.

In practice, we truncate the series representation to suitable order  $N$  and we require that the invariance condition holds up to a tolerance  $\tau_{\text{tol}}$ . Then, the invariance condition will hold for  $X$  in a domain of radius  $r_{\mathbf{p}_1}$  around the fixed point  $\mathbf{p}_1$  (similarly, for  $\mathbf{x}_0$  we obtain  $r_{\mathbf{x}_0}$ ). Typical values used in the computations are  $N = 150$  and  $\tau_{\text{tol}} = 10^{-40}$ . The local domain size depends on the parameter  $a_L$  in the system. As an example, for  $a_L = 0.15$  one obtains  $r_{\mathbf{p}_1} = 265$  and  $r_{\mathbf{x}_0} = 1470$ .

Once the local representations  $K^{p_1}$  and  $K^{x_0}$ , of  $W^u(\mathbf{p}_1)$  and  $W^s(\mathbf{x}_0)$  respectively, are obtained we extend the  $W^u(\mathbf{p}_1)$  up to  $\Sigma = \{p_2 = K_3^{x_0}(r_{x_0}, 0)\}$ , where  $K_3^{x_0}$  denotes the 3rd component of  $K^{x_0}$  (the one corresponding to the  $p_2$ -variable). This is done by integrating the Eq. (26) using a Taylor method, which turns out to be an appropriate time-stepper for the high precision computations required. Assume that  $K^{p_1}(z_1, z_2) \in \mathbb{R}^4$  is a point such that the transported one  $\hat{K}^{p_1}(z_1, z_2) \in \Sigma$  is close to a zero of  $F(s_1, s_2, z_1, z_2) = K^{x_0}(s_1, s_2) - \hat{K}^{p_1}(z_1, z_2)$ ,  $F : \mathbb{R}^4 \rightarrow \mathbb{R}^4$ . Then we refine

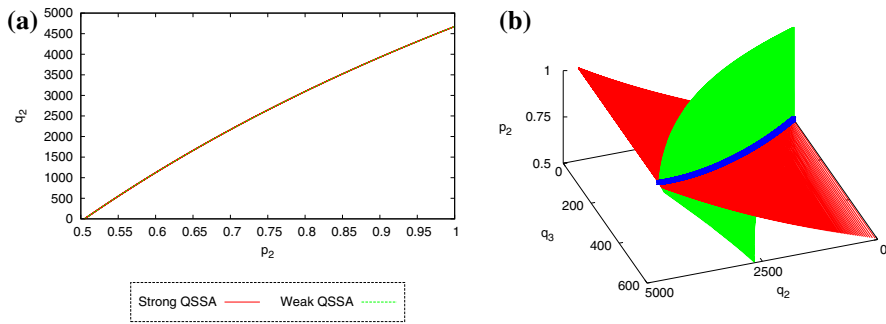


**Fig. 6** **a** Projection on the  $(p_2, q_2)$ -plane of the heteroclinic connection between the metastable state and the stochastic extinction, computed with the strong QSSA and the weak QSSA.  $a_L = a_L^s$ . **b** 3D plot of the stable invariant manifold of the stochastic extinction (red), unstable invariant manifold of the metastable state (green) and the heteroclinic connection between these two points (blue), given by the intersection between both invariant manifolds, computed with the weak QSSA.  $a_L = a_L^s$

this initial condition, using a Newton method and we obtain a point of the heteroclinic orbit as a zero of  $F$ . Note that this requires to integrate the first variational equations. See Simó (1990) for further details.

Similar computations for a 2-dof system as well as for a 4D map were carried out in Gelfreich et al. (2013), where further technical details on the parametrization method and the computation of homo/heteroclinic trajectories can be found. For a recent overview of the parametrization method for computation of invariant manifolds in different contexts see Haro et al. (2016).

In Fig. 6a we show the heteroclinic connection, projected on the  $(p_2, q_2)$  plane, computed with the strong QSSA and the weak QSSA, using the numerical methods explained in this section. We find that there is an excellent agreement between both approximations. In particular, this justifies the usage of the strong QSSA for the computations. In Fig. 6b we show a 3D representation of  $W^u(\mathbf{p}_1)$  and  $W^s(\mathbf{x}_0)$  for the Weak QSSA.

### Appendix 3: Numerical fit of $A$ and $B$

It is clear that as  $N_c \rightarrow \infty$  ( $\Omega \rightarrow \infty$ ) the solution of the semi-classical approximation tends to the exact solution of Eq. (1), and we can use this fact in our advantage to determine  $A$  and  $B$ . We also have to notice that we can determine analytically  $C$ , as it is the integral of the action along the heteroclinic connection. A direct fit of a function of the form

$$f(N_c) = AN_c^B \exp(CN_c)$$

can be very unstable. We rather analyse

$$g(x) = \frac{1}{N_c} \log f(N_c) = \hat{A}x + \hat{B}x \log(x) + \hat{C},$$

with  $x = \frac{1}{N_c}$ , which is more favourable, since first we are interested in  $C$ , therefore we want to have  $C$  alone with small terms suppressed by  $N_c$ . Our procedure is as follows,

1. Given a  $a_L$  we select an initial  $N_c$  and we compute  $\tau$  using stochastic simulations (the multi-scale stochastic simulation employed to perform this simulations is explained later).
2. Save  $\epsilon_{N_c} = \frac{1}{N_c}$  and  $\delta_{N_c} = \epsilon \log\left(\frac{1}{\tau}\right)$ . Increase  $N_c$  and go to 1 until we have some values of  $(\epsilon_{N_c}, \delta_{N_c})$ .
3. Using an implementation of the non-linear least-squares (NLLS) Levenberg-Marquardt algorithm (Nocedal and Wright 2006) fit  $g(x) = \hat{A}x + \hat{B}x \log(x) + \hat{C}$  via  $\hat{A}$ ,  $\hat{B}$ ,  $\hat{C}$  where  $x = \log(\delta_{N_c})$  and the right-hand term is  $\epsilon \delta_{N_c}$  with some of the higher values of  $N_c$  we have.
4. If  $|\hat{C} - C| > \text{tol}$ , where  $C$  is the one obtained analytically, increase  $N_c$  and go to 1.
5. If  $|\hat{C} - C| < \text{tol}$  we choose  $\hat{C} = C$  and we fit again via  $\hat{A}$  and  $\hat{B}$ .
6. As we can expect  $B$  of the form  $B = \pm \frac{n}{2}$  with  $n \in \mathbb{N}$ , we choose  $B$  as the closest number of this form to  $B$ .
7. Finally we fit again just via  $A$  to check robustness of the previous fit and get a better approximation of  $A$ .
8. As we are interested in  $\Omega = 5000$  ml, the mean extinction time, obtained with the semi-classical approximation is,  $\tau_s = -\left(g\left(\frac{V_c}{5000}\right) \frac{5000}{V_c}\right)$ .

Note that we expect  $B$  to take this form, since this system exhibits the so-called Stokes phenomenon (Arnol'd 1989). Therefore it is natural to expect that there is a singularity in the complex space which is a pole. For instance, for the Branching-Binary Annihilation-decay process, it has been proven that  $B = \frac{1}{2}$  (Assaf and Meerson 2006, 2007, 2010). Numerically we have observed that  $B$  approaches  $\frac{1}{2}$  (independently of  $a_L$ ). To obtain analytic expressions for  $A$  and  $B$  requires a careful analysis of the related Stokes phenomenon (Assaf and Meerson 2010). This is postponed for future work.

## References

- Alarcón T (2014) Stochastic quasi-steady state approximations for asymptotic solutions of the chemical master equation. *J Chem Phys* 140:184109
- Alarcón T, Jensen HJ (2011) Quiescence: a mechanism for escaping the effects of drug on cell populations. *J R Soc Interface* 8(54):99–106
- Alarcón T, Page KM (2007) Mathematical models of the vegf receptor and its role in cancer therapy. *J R Soc Interface* 4:283–304
- Arnol'd VI (1989) *Mathematical methods of classical mechanics*, vol 60. Springer, New York
- Assaf M, Meerson B (2006) Spectral theory of metastability and extinction in birth-death systems. *Phys Rev Lett* 97(20):200602
- Assaf M, Meerson B (2007) Spectral theory of metastability and extinction in a branching-annihilation reaction. *Phys Rev E* 75(3):031122
- Assaf M, Meerson B (2010) Extinction of metastable stochastic populations. *Phys Rev E* 81:021116
- Assaf M, Meerson B, Sasorov PV (2010) Large fluctuations in stochastic population dynamics: momentum-space calculations. *J Stat Mech*:P07018

- Batut C, Belabas K, Bernardi D, Cohen H, Olivier M (1995) Users' guide to PARI/GP. <http://pari.math.u-bordeaux.fr/>
- Bohil AB, Robertson BW, Cheney RE (2006) Myosin-x is a molecular motor that functions in filopodia formation. *Proc Nat Acad Sci* 103(33):12411–12416
- Cabr   X, Fontich E, De La Llave R (2005) The parameterization method for invariant manifolds iii: overview and applications. *J Differ Equations* 218(2):444–515
- Cao Y, Gillespie D, Petzold L (2005) Multiscale stochastic simulation algorithm with stochastic partial equilibrium assumption for chemically reacting systems. *J Comput Phys* 206(2):395–411
- Chomont N, El-Far M, Ancuta P, Trautmann L, Procopio FA, Yassine-Diab B, Boucher G, Boulassel M-R, Brenchley JM, Schacker TW, Hill BJ, Ghattas DCDG, Routy J-P, Haddad EK, Sekaly R-P (2009) HIV reservoir size and persistence are driven by T cell survival and homeostatic proliferation. *Nature Med* 15:893–901
- Chun T-W, Carruth L, Finzi D, Shen X, DiGiuseppe JA, Taylor H, Hermankova M, Chadwick K, Margolick J, Quinn TC, Kuo Y-H, Brookmeyer R, Zeiger MA, Barditch-Crovo P, Siliciano RF (1997) Quantification of latent tissue reservoirs and total body viral load in HIV-1 infection. *Nature* 387:183–188
- Chun TW, Finzi D, Margolick J, Chadwick K, Schwartz D, Siliciano RF (1995) In vivo fate of HIV-1-infected T cells: quantitative analysis of the transition to stable latency. *Nat Med* 1:1284–1290
- Conway JM, Coombs D (2011) A stochastic model of latently infected cell reactivation and viral blip generation in treated HIV patients. *PLoS Comput Biol* 7:e1002033
- de la Cruz R, Guerrero P, Spill F, Alarc  n T (2014) The effects of intrinsic noise on the behaviour of bistable systems in quasi-steady state conditions (submitted)
- Doering CR, Sargsyan KV, Sander LM (2005) Extinction times for birth-death processes: exact results, continuum asymptotics, and the failure of the fokker-planck approximation. *Multiscale Model Simul* 3:283
- Dykman MI, Mori E, Ross J, Hunt PM (1994) Large fluctuations and optimal paths in chemical kinetics. *J Chem Phys* 100:5735–5750
- Dykman MI, Schwartz IB, Landsman AS (2008) Disease extinction in the presence of random vaccination. *Phys Rev Lett* 101:078101
- Elgart V, Kamenev A (2004) Rare event statistics in reaction-diffusion systems. *Phys Rev E* 70:041106
- Freidlin MI, Wentzell AD (1998) Random perturbations of dynamical systems, vol. 260 of *grundlehren der mathematischen wissenschaften (fundamental principles of mathematical sciences)*
- Gardiner CW (2009) *Stochastic methods*. Springer, Berlin
- Gelfreich V, Sim   C, Vieiro A (2013) Dynamics of 4D symplectic maps near a double resonance. *Phys D* 243(1):92–110
- Gillespie DT (1976) A general method for numerically simulating the stochastic time evolution of coupled chemical reactions. *J Comput Phys* 22(4):403–434
- Goldstein H (1980) *Classical mechanics*
- Gottesman O, Meerson B (2012) Multiple extinction routes in stochastic population models. *Phys Rev E* 85:021140
- Gray C, Karl G, Novikov V (2004) Progress in classical and quantum variational principles. *Reports Progress Phys* 67(2):159
- Gray C, Taylor EF (2007) When action is not least. *Am J Phys* 75(5):434–458
- Haro A, Canadell M, Figueras J, Luque A, Mondelo J (2016) The parameterization method for invariant manifolds: from rigorous results to effective computations. Springer, New York
- Herz AVM, Bonhoefer S, Anderson RM, May RM, Nowak MA (1996) Viral dynamics in vivo: limitations on estimates of intracellular delay and virus decay. *Proc Natl Acad Sci* 93:7247–7251
- Ho DD, Neumann AU, Perelson AS, Chen W, Leonard JM, Markowitz M (1995) Rapid turnover of plasma virions and CD4 lymphocytes in HIV-1 infection. *Nature* 373:123–126
- Ho DD, Rota TR, Hirsch MS (1986) Infection of monocyte/macrophages by human T lymphotropic virus type III. *J Clin Invest* 77:1712–1715
- Jones LE, Perelson AS (2007) Transient viremia, plasma viral load and reservoir replenishment in HIV-infected patients on antiretroviral therapy. *J Acquir Immune Defic Syndr* 45:483–493
- Jorba   , Zou M (2005) A software package for the numerical integration of ODEs by means of high-order Taylor methods. *Exp Math* 14(1):99–117
- Kamenev A, Meerson B (2008) Extinction of an infectious disease: a large fluctuation in a non-equilibrium system. *Phys Rev E* 77:061107

- Katlama C, Deeks SG, Autran B, Martinez-Picado J, van Luzen J, Rouzioux C, Miller M, Vella S, Schmitz JE, Ahlers J, Richman DD, Sekaly RP (2013) Barriers to a cure for HIV: new ways to target and eradicate HIV-1 reservoirs. *Lancet* 381:2109–2117
- Kent SJ, Reece JC, Petravic J, Martyushev A, Kramski M, Rose RD, Cooper DA, Kelleher AD, Emery S, Cameron PU, Lewin SR, Davenport MP (2013) The search for an HIV cure: tackling latent infection. *Lancet Infect Dis* 13:614–621
- Kepler TB, Perelson AS (1998) Drug concentration heterogeneity of drug resistance facilitates the evolution of drug resistance. *Proc Natl Acad Sci* 95:11514–11519
- Khasin M, Dykman MI (2009) Extinction rate fragility in population dynamics. *Phys Rev Lett* 103:068101
- Khasin M, Dykman MI, Meerson B (2010) Speeding up disease extinction with a limited amount of vaccine. *Phys Rev E* 81:051925
- Kim H, Perelson AS (2006) Viral and latent reservoir persistence in HIV-1-infected patients on therapy. *PLoS Comp Biol* 2:e135
- Kubo R, Matsou K, Kitahara K (1973) Fluctuations and relaxation of macrovariables. *J Stat Phys* 9:51–96
- Landau L, Lifshitz E (1976) Course of theoretical physics. Vol. 1. Mechanics (trans: Russian by Skyes JB, Bell JS). Pergamon Press, Oxford, New York, Toronto, ON
- Markowitz M, Louie M, Hurley A, Sun E, Mascio MD, Perelson AS, Ho DD (2003) A novel antiviral intervention results in more accurate assessment of human immunodeficiency virus type 1 replication dynamics and t-cell decay in vivo. *J Virol* 77:5037–5038
- Nocedal J, Wright SJ (2006) Numerical optimization, 2nd edn. Springer, New York
- Ovaskainen O, Meerson B (2010) Stochastic models of population extinction. *Trends Ecol. Evol.* 25:646–652
- Perelson AS, Essunger P, Cao Y, Vesanen M, Hurley A, Saksela K, Markowitz M, Ho DD (1997) Decay characteristics of HIV-1-infected compartments during combination therapy. *Nature* 387:188–191
- Perelson AS, Neumann AU, Markowitz M, Leonard JM, Ho DD (1996) HIV-1 dynamics in vivo: virion clearance rate, infected cell life-span, and viral generation time. *Science* 271:1582–1586
- Pierson T, McArthur J, Siciliano RF (2000) Reservoirs for HIV-1: mechanisms for viral persistence in the presence of antiviral immune response and antiretroviral therapy. *Annu Rev Immunol* 18:665–708
- Rong L, Perelson AS (2009) Modeling latently infected cell activation: viral and latent reservoir persistence, and viral blips in HIV-infected patients on potent therapy. *PLoS Comput Biol* 5:e1000533
- Rong L, Perelson AS (2009) Modelling HIV persistence, the latent reservoir, and viral blips. *J Theor Biol* 260:308–331
- Schwartz IB, Billings L, Dykman MI, Landsman AS (2009) Predicting extinction rates in stochastic epidemic models. *J Stat Mech*:P01005
- Shan L, Deng K, Shroff NS, Durand CM, Rabi SA, Yang H-C, Zhang H, Margolick JB, Blankson JN, Siciliano RF (2012) Stimulation of HIV-1-specific cytolytic T lymphocytes facilitates elimination of latent viral reservoir after virus reactivation. *Immunity* 36:491–501
- Siliciano JD, Kajdas J, Finzi D, Quinn TC, Chadwick K, Margolick JB, Kovacs C, Gange SJ, Siliciano RF (2003) Long-term follow-up studies confirm the stability of the latent reservoir for hiv-1 in resting CD4+ T cells. *Nat Med* 9:727–728
- Simó C (1990) On the analytical and numerical approximation of invariant manifolds. In: *Les Méthodes Modernes de la Mécanique Céleste. Modern methods in celestial mechanics vol. 1*, pp 285–329
- Trono D, Lint CV, Rouzioux C, Verdin E, Barre-Sinoussi F, Chun T-W, Chomont N (2010) HIV persistence and the prospect of long-term drug-free remissions for HIV-infected individuals. *Science* 329:174–180
- Van Kampen NG (2007) Stochastic processes in physics and chemistry. Elsevier, The Netherlands
- Ward MJ (1998) Exponential asymptotics and convection-diffusion reactions models. In: *Analysing multiscale phenomena using singular perturbation methods, Proceedings of Symposia in Applied Mathematics*, vol. 56, pp 151–184. AMS Short Courses
- Wei X, Ghosh SK, Taylor ME, Johnson VA, Emmini EA, Deutsch P, Lifson JD, Bonhoeffer S, Nowak MA, Hahn BH, Saag MS, Shaw GM (1995) Viral dynamics in human immunodeficiency virus type 1 infection. *Nature* 373:117–122
- Zhang Z-Q, Schuler T, Zupancic M, Wietgreffe S, Staskus KA, Reimann KA, Reinhart TA, Rogan M, Cavern W, Miller CJ, Veazey RS, Notermans D, Little S, Danner SA, Richman DD, Havlir D, Wong J, Jordan HL, Schacker TW, Racz P, Tenner-Racz K, Letvin NL, Wolinsky S, Haase AT (1999) Sexual transmission and propagation of SIV and HIV in resting and activated CD4+ T Cells. *Science* 286:1712–1715